Magnetic and transport properties of Fe-Ag granular multilayers

M. Csontos,[1] J. Balogh,[2] D. Kaptás,[2] L. F. Kiss,[2] A. Kovács,[3] and G. Mihály[1]
[1]*"Electron Transport in Solids" Research Group of the Hungarian Academy of Sciences and Department of Physics, Budapest University of Technology and Economics, 1521 Budapest, P.O. Box 91, Hungary*
[2]*Research Institute for Solid State Physics and Optics, 1525 Budapest, P.O. Box 49, Hungary*
[3]*Research Institute for Technical Physics and Materials Sciences, 1525 Budapest, P.O. Box 49, Hungary*
(Received 2 June 2005; revised manuscript received 3 March 2006; published 10 May 2006)

Results of magnetization, magnetotransport, and Mössbauer spectroscopy measurements of sequentially evaporated Fe-Ag granular composites are presented. The strong magnetic scattering of the conduction electrons is reflected in the sublinear temperature dependence of the resistance and in the large negative magnetoresistance. The simultaneous analysis of the magnetic properties and the transport behavior suggests a bimodal grain size distribution. A detailed quantitative description of the unusual features observed in the transport properties is given.

DOI: 10.1103/PhysRevB.73.184412 PACS number(s): 75.47.De, 75.70.Cn, 75.20.En, 73.43.Qt

I. INTRODUCTION

As promising candidates for magnetic recording and sensor applications heterogeneous magnetic materials, i.e., multilayer structures[1,2] of alternating ferromagnetic and nonmagnetic layers and granular composites[3–6] have been studied widely in the last two decades. The giant magnetoresistance (GMR) in these systems have been explained by elastic scattering of the conduction electrons on magnetic moments of differently aligned magnetic entities. Gittleman *et al.* have shown that in superparamagnetic granular alloys this consideration leads to a magnetoresistance proportional to the square of the magnetization.[7] Deviations from this relation has been attributed to the size distribution of the magnetic scatterers[8,9] and interactions between these scatterers.[10–12] Various assumptions on the form of the size distribution have been made in order to obtain a phenomenological description of the GMR phenomena in different granular systems.

In this paper we present a detailed study of the magnetic and magnetotransport properties of a Fe-Ag granular multilayer sample and deduce the characteristic features of the size distribution of the Fe grains from these measurements. It is especially important in the case of Fe-Ag system, because x-ray diffraction methods or transmission electron microscopy (TEM), as it will be shown, cannot identify Fe grains of a few nm size. The magnetic properties will be studied in a broad temperature and magnetic field range by three different methods. The macroscopic magnetization was measured by a superconducting quantum interference device (SQUID) up to 5 T and by anomalous Hall effect up to 12 T applied field. The distribution of the local magnetic fields was studied by Mössbauer spectroscopy. These measurements can be rather well characterized by supposing interaction free superparamagnetic particles of uniform grain size. The observed unusual sublinear temperature dependence ($d^2R/dT^2<0$) of the resistivity will be described by electron scattering on magnetic clusters of a much smaller size. Finally, the large nonsaturating negative magnetoresistance will be discussed in the framework of a bimodal size distribution with the above two characteristic sizes of the grains and the clusters. Deviation from the proportionality of the magnetoresistance and the square of the magnetization observed for large applied fields is explained by the small fraction of Fe atoms in the clusters, as indicated by the Mössbauer results.

II. GRANULAR MULTILAYER STRUCTURE

The Fe-Ag multilayer samples were prepared by sequential vacuum evaporation in a base pressure of 10^{-7} Pa onto Si(111) single crystal substrates at room temperature. The mass of the deposited material was measured by a quartz oscillator and the nominal layer thickness was calculated using the bulk density of Fe and Ag. Most data shown in this paper were obtained on a specimen, A, prepared with the following sequence:

$$\text{(A) } [\text{Ag}(2.6\text{ nm})/\text{Fe}(0.2\text{ nm})]_{75}/\text{Ag}(2.6\text{ nm})$$

where the rectangular brackets and the subscripts to them indicate the basic unit of the multilayer and the number of repetitions.

The absence of peaks in the x-ray reflectivity[13] when the Fe layer thickness is less than ≈ 1 nm is attributed to discontinuities of the Fe layers. This limit of the continuous layer regime is quite similar to that observed in other multilayer systems[14–16] composed of transition metals with immiscible nonmagnetic elements and these kind of discontinuous multilayers are often referred to as granular multilayers.[17]

Structural characterization of granular multilayer samples by x-ray diffraction indicated a nanometer scale grain size of the constituents (for details see Ref. 13), however, due to the strong overlap between the diffraction lines of bcc-Fe and fcc-Ag, a quantitative evaluation of the size of the magnetic Fe grains was not possible.

Direct determination of the Fe grain size was also attempted by transmission electron microscopy (TEM). Earlier studies on co-deposited Fe-Ag granular alloys[18] already indicated that several problems might obstacle this investigation. For small Fe concentrations (around 10 at %) the Fe atoms were found to be dispersed in the fcc Ag matrix or in

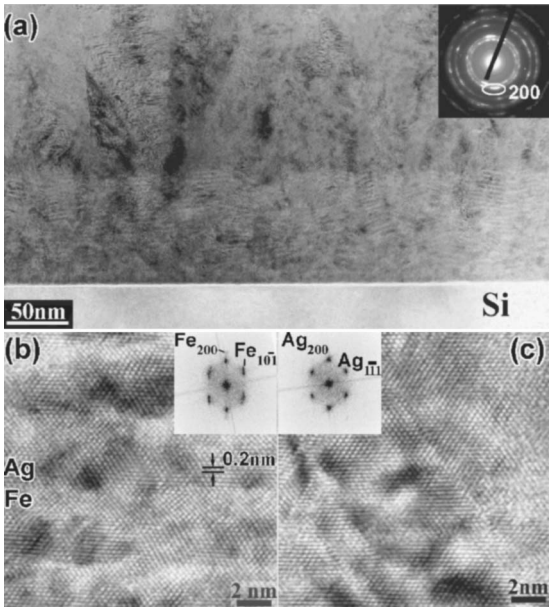

FIG. 1. Cross-sectional TEM analysis of the combined Fe-Ag sample. (a) The bright field image shows the separable bottom and upper part of the sample. The slight 200 texture of the sample is indicated on SAED pattern by the inserted ellipse. (b) The HRTEM image from the bottom part with Ag(2.6 nm) and Fe(1.5 nm) layers. The FFT image (inset) indicates both Ag and Fe reflections. (c) The HRTEM image from the top part of the sample. The FFT image contains only Ag reflections.

disordered regions and could not be distinguished. Grain growth starts at relatively low temperatures[19] which makes sample preparation difficult and for this reason TEM studies generally use special microgrid substrates. Both the preparation method and the substrate material can influence the structure of the sample making comparison to other measurements ambiguous. To overcome this problem a careful sample preparation and a combined sample structure was chosen. The sample studied was grown on a Si(111) substrate with the following sequence:

$$\text{Si substrate/Ag(2.6 nm)/[Ag(2.6 nm)/Fe(1.5 nm)]}_{25}\text{/}$$
$$\text{[Ag(2.6 nm)/Fe(0.2 nm)]}_{75}\text{/Ag(2.6 nm)}.$$

The top part agrees with the structure of sample A used for the present magnetic and transport studies, while the bottom part contains thicker (1.5 nm) Fe layers with unvaried Ag layer thickness. This combination provides a better understanding of the structure of the Fe layers and the top part was shown to have the same magnetic properties[20] as the simple granular multilayer sample. The cross sectional sample preparation was made by low energy (200 eV) and low angle ($<3°$) Ar^+ ion milling to reduce sample damage and a liquid N_2 cooled sample holder was applied to avoid heating of the specimen during sample preparation. Images of high resolution transmission electron microscopy (HRTEM) were obtained using a JEOL 3010 UHR microscope, with the point resolution of 0.17 nm. Figure 1 shows images taken for the full cross section with normal resolution [Fig. 1(a)], and the HRTEM images of the bottom [Fig. 1(b)] and the top [Fig. 1(c)] part of the sample. The combined sample structure is visible in the full cross section image. The selected area electron diffraction (SAED) indicates a 200 texture of the sample. The layered structure of the bottom part is clearly separated from the more homogeneous upper portion of the sample. The layers in the bottom part are rather wavy and a columnar growth structure extending to the upper sample region can be observed. The lattice fringe image of Fig. 1(b) shows that the Fe layers grew epitaxially on the Ag layers with (100)Fe‖ (100)Ag, [010]Fe‖ [011]Ag orientational relationship. The fast Fourier transformation (FFT) images taken from the HREM images are also shown and confirm the existence of both the fcc-Ag and the bcc-Fe phase in the case of the bottom part. Contrary to the clearly separated Ag and Fe layers, the Fe granules cannot be identified in the HRTEM image taken from the top part of the sample [Fig. 1(c)] and bcc-Fe spots cannot be observed in the FFT image. The high number of dislocations probably indicates the Fe granules embedded in the Ag matrix, but determination of the grain size distribution and the morphology are obviously hindered by an fcc or fct structure of the small grains. The critical thickness of the bcc-Fe structure formation should be below 1.5 nm, that is quite close to the continuous layer regime.

III. MAGNETIC PROPERTIES

The magnetic structure was examined by a Quantum Design MPMS-5S superconducting quantum interference device (SQUID) up to $B=5$ T and by the transmission Mössbauer spectroscopy applying a standard constant acceleration spectrometer and a Janis cryostat equipped with a $B=7$ T superconducting magnet. For the latter purpose the sample has been removed from the substrate and folded up to achieve an appropriate thickness for transmission measurements.

The ^{57}Fe Mössbauer spectra of sample A taken at several temperatures are shown in Fig. 2. The room temperature spectrum contains a paramagnetic doublet with a large isomer shift relative to α-Fe (0.18 mm/s) and a quadrupole splitting (0.45 mm/s) characteristic to a system of small Fe clusters embedded in an Ag matrix.[21] The low temperature spectra show that the sample is superparamagnetic (SPM) and as the magnetic clusters gradually freeze below the blocking temperature (around 50 K), the six-line pattern characteristic to the Zeeman splitting of the nuclear levels of ^{57}Fe appears. At $T=4.2$ K the paramagnetic fraction is absent, but the spectral lines are much broader and the hyperfine parameters are different from those of bulk bcc-Fe. The 4.2 K spectrum could be fitted with a distribution of hyperfine fields[22] with an average value, $H_{av}=34.7$ T and standard deviation, $\sigma_H=2.4$ T. The individual six-line patterns of the fitted distribution are shown in Fig. 2. It is clearly visible that the strong asymmetry of the overall spectrum is due to a strong correlation of the magnetic splitting and the isomer shift: The smaller the magnetic splitting of the sextett, the larger positive isomer shift belongs to it.

It is worth noting that the intensity ratios of the six lines indicate a significant spontaneous alignment of the magnetic moments. The intensity of the six lines of a sextet

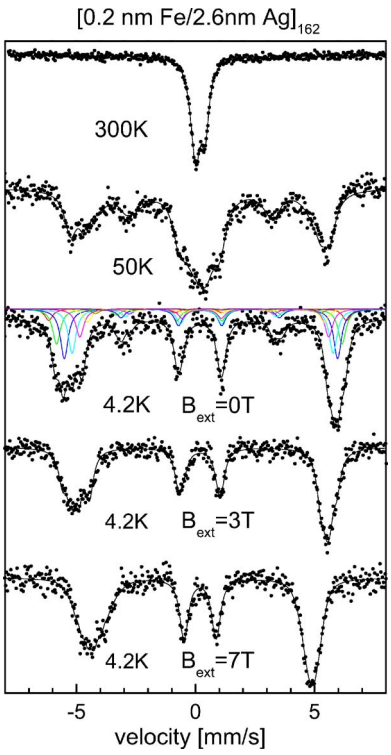

FIG. 2. (Color online) Transmission Mössbauer spectra of sample A at various temperatures and at T=4.2 K in various magnetic fields. For the T=4.2 K, B_{ext}=0 T spectrum the individual six-line patterns of the fitted distribution are also plotted.

is distributed as $3:I_{2-5}:1:1:I_{2-5}:3$, where $I_{2-5}=4\sin^2\Theta/(1+\cos^2\Theta)$ is the intensity of the m=0 transitions, and Θ is the angle between the direction of the gamma-ray (perpendicular to the sample plane) and the magnetic moment. In case of a random distribution of the magnetization directions I_{2-5}=2. The observed small intensity, I_{2-5}=0.5, indicates a close-to-perpendicular alignment of the magnetic moments with respect to the sample plane. Applying a magnetic field perpendicular to the sample plane could fully align the moments parallel to the field, as it is indicated by the I_{2-5}=0 intensity.

The spectra measured in external magnetic field were also fitted with a distribution of the hyperfine fields and the parameters obtained are: H_{av}=32.5 and 27.8 T and σ_H=2.3 and 2.4 T for B_{ext}=3 and 7 T. The external magnetic field does not affect the width of the distribution indicating that it is not due to relaxation of the magnetic moments. The broad spectral lines of the observed sextet result from a distribution of the Fe neighborhoods, which can be due both to the large number of surface atoms in small grains and to nonequilibrium mixing of the elements[23] during the growth process. The field-independent width and the decrease of the observed average hyperfine field in external field indicate the ferromagnetic alignment of the magnetic grains. The hyperfine field of a ferromagnet is decreased by the applied field, since it is oriented antiparallel to the magnetic moment. We note that at 4.2 K the statistical errors allow an SPM fraction containing less than 2% of the Fe atoms.

The freezing of the superparamagnetic moments—seen in the Mössbauer spectra—also appears in the temperature dependence of the low field susceptibility measured by the SQUID. Figure 3 shows the results after cooling the sample either in zero or in 1 mT permanent magnetic field. Our granular multilayer sample (prepared by sequential vacuum evaporation) exhibits a rather sharp cusp of the ZFC curve at T_B=40 K, almost coinciding with the FC-ZFC irreversibility temperature.

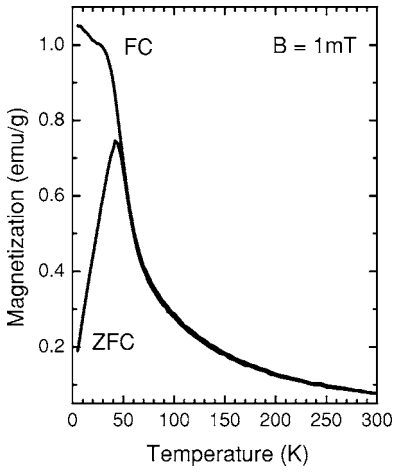

FIG. 3. Zero field cooled (ZFC) and field cooled (FC) magnetization as a function of temperature.

The magnetization curves measured up to B=5 T applied field at several temperatures are shown in Fig. 4. The curves could be quite well fitted with a single Langevin function, L, as expected for a superparamegnetic system of uniform grains:

$$M(T,B) = M_s(T)L(T,B)$$

$$L(T,B) = \coth\frac{\mu_G B}{k_B T} - \frac{k_B T}{\mu_G B}, \tag{1}$$

where μ_G is the magnetic moment of the grains and $M_s(T)$ is the saturation magnetization. The magnetic moment deduced from the fits is shown in the inset of Fig. 3 as a function of

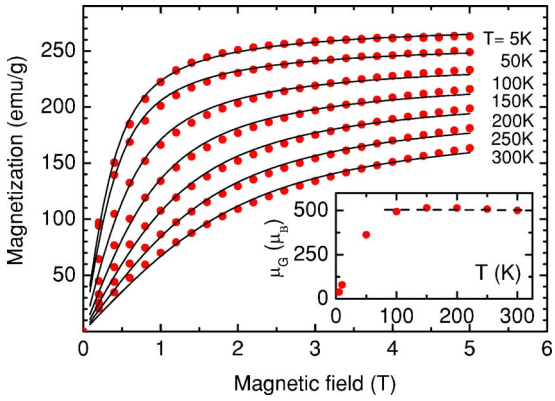

FIG. 4. (Color online) Magnetization measured by a SQUID magnetometer up to B=5 T magnetic field at various temperatures. The solid lines correspond to Langevin-fits, the characteristic magnetic moments determined from the fits at various temperatures are shown in the inset.

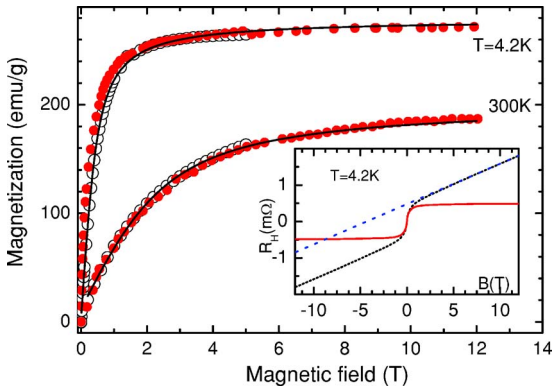

FIG. 5. (Color online) Field dependence of the magnetization obtained from anomalous Hall effect data (red dots) normalized to the SQUID measurements (open black circles). The continuous lines are the same Langevin fits as in Fig. 3. The inset shows the measured Hall-resistance (black dots), and the separation of the linear Lorentz-term (blue curve) and the anomalous Hall signal (red curve).

the temperature. Above $T \approx 100$ K we found $\mu_G = 500\ \mu_B$, indicating that the bulk magnetic properties are mainly determined by grains of about 1.8 nm average size and the effect of the size distribution is negligible. At temperatures close to or below the blocking temperature of $T_B = 40$ K the magnetization can still be described with a Langevin function, but with an apparent grain size gradually decreasing by lowering the temperature. This feature is quite general for granular systems and formally can be treated by a Langevin function with modified argument accounting for an effective interaction.[12]

The field dependence of the magnetization was investigated in an extended field range by means of the anomalous Hall-effect. The Hall-resistivity in a magnetic material can be expressed as

$$\rho_{\mathrm{Hall}} = R_0 B + \beta(B) P(B) \approx R_0 B + R_A M(B) \qquad (2)$$

The first (linear) term is the normal Hall-resistivity arising from the Lorenz-force. The second term is the anomalous Hall-resistivity which is expected to be proportional to the spin polarization of the carriers (P), independently of its microscopic origin (typically spin-dependent asymmetric scattering or Barry phase effects). The right hand side of the equation assumes that the spin polarization of the carriers is proportional to the macroscopic magnetization, $P(B) \propto M(B)$, which is fulfilled for common laboratory magnetic fields. In our experiments fields up to $B = 12$ T were applied perpendicular to the sample surface and a large Hall-signal was detected due to the advantageous sample geometry. The Hall resistance was obtained from the $V(B) = -V(-B)$ antisymmetrical component of the measured voltage. (The voltage drop due to the unavoidable misalignment of the side contacts results in a symmetrical component.) The Lorentz-term, linear in B was separated as shown for $T = 4.2$ K in the inset of Fig. 5. The magnetization was deduced from the anomalous Hall resistance by scaling the low field data to the SQUID results, as shown in Fig. 5 for $T = 4.2$ and 300 K. The

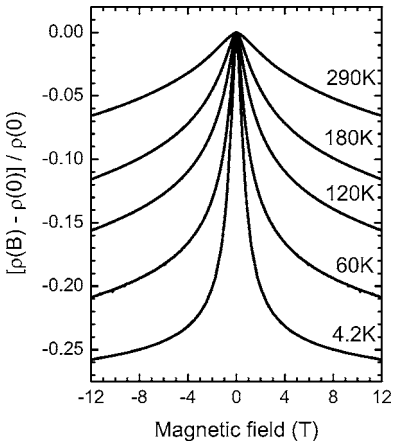

FIG. 6. Magnetic field dependence of the resistivity at various temperatures.

overlapping SQUID and anomalous Hall data below $B = 5$ T verify the validity of Eq. (2), while the solid lines demonstrate that the high-field behavior of the magnetization follows the extension of the Langevin fits obtained from (the more accurate) SQUID experiments.

IV. TEMPERATURE DEPENDENCE OF THE MAGNETIC SCATTERING

The longitudinal magnetotransport measurements have been performed in the current-in-plane arrangement by four contact method. The observed large negative magnetoresistance is shown in Fig. 6 for various temperatures. We found that the parallel ($H \| I$) and the transversal ($H \perp I$) magnetoresistance coincide; the absence of any anisotropic component is characteristic to the GMR phenomenon in granular systems.[4]

The temperature dependence of the resistivity is displayed in Fig. 7 both for zero and 12 T magnetic fields. The curves are normalized to the saturated value measured at $B = 12$ T in the $T \to 0$ K limit. Contrary to ordinary metallic systems, the resistivity is sublinear above 40 K in both cases. Similar observation was reported by Milner *et al.* for granular Co-Ag films,[6] but only in the presence of a high magnetic field. As discussed later in detail, the above qualitative feature of the zero field temperature dependencies signifies the presence of an extremely strong magnetic scattering in our samples.

It is also important to emphasize that the magnetoresistance curves do not saturate even in high magnetic fields and at low temperatures, where the magnetization seems already to be saturated. This indicates that significant magnetic scattering takes place at magnetic entities much smaller than the typical grain size which determines the macroscopic magnetization. It is well known that the scattering amplitude of ferromagnetic grains embedded in a nonmagnetic metallic matrix is size dependent and the contribution of the smaller clusters is strongly enhanced.[5] The magnetic moments of these smaller clusters are harder to rotate by an applied magnetic field thus the saturation of the magnetoresistance is slower than that of the net magnetization arising dominantly from the larger grains.[24]

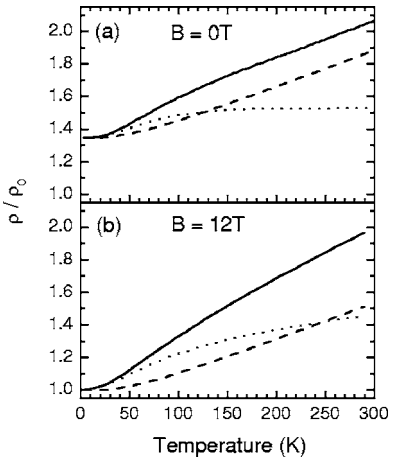

FIG. 7. Resistivity vs temperature in zero (a) and 12 T magnetic fields (b). The solid lines are the experimental data, dashed lines indicate the magnetic field independent phonon scattering, as calculated from the high temperature slope of ρ(T). The dotted curves are the differences of the former two (shifted upwards by the residual resistivity), and are attributed to the temperature-dependent magnetic scattering on small Fe clusters.

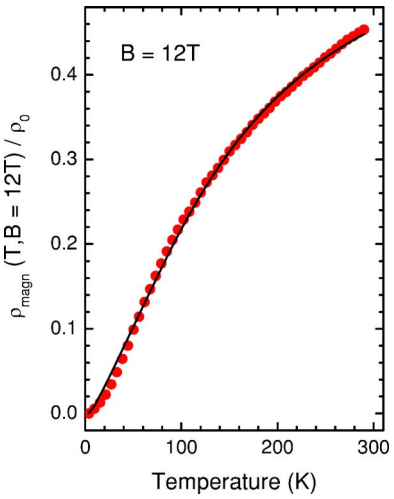

FIG. 8. (Color online) Temperature dependence of the resistivity contribution attributed to magnetic scattering on tiny Fe clusters in $B=12$ T magnetic field. Symbols are experimental data after subtracting the phonon contribution as shown in Fig. 7, solid curves are calculated from Eq. (5) with fitting parameter $S=16.6\ \mu_B$.

In order to separate the magnetic scattering process we assume that the Matthiessen-rule can be applied, i.e., the resistivity is composed of 3 terms:

$$\rho(T,B) = \rho_0 + \rho_{\mathrm{ph}}(T) + \rho_{\mathrm{magn}}(T,B). \tag{3}$$

Here ρ_0 denotes the residual resistivity, $\rho_{\mathrm{ph}}(T)$ is the contribution arising from the phonon scattering, and the remaining part is attributed to the magnetic scattering. The residual resistivity corresponds to the $T\rightarrow 0$, $B\rightarrow\infty$ value where both the phonon and the magnetic scattering freeze out. In the followings we often use it as a normalization factor, with the approximation of $\rho_0 \approx \rho(T=4.2\ \mathrm{K}, B=12\ \mathrm{T})$.

The separation of the magnetic and phonon scattering requires further consideration. In a granular system the magnetic scattering depends on the correlation between the localized magnetic moments of the grains, $\langle \boldsymbol{\mu}_i \boldsymbol{\mu}_f \rangle$, while a conduction electron is scattered from $\boldsymbol{\mu}_i$ to $\boldsymbol{\mu}_f$ within its spin-diffusion length.[7] In zero magnetic field, well above the blocking temperature the magnetic moments of the grains (including the large grains) are fully disordered. Under these circumstances no temperature dependence is expected from the magnetic scattering, at least as long as the spin diffusion length is large enough. We assume that at high temperatures the temperature dependence of the resistivity arises solely from the phonon contribution,

$$\rho_{ph}(T) = a_1 \left(\frac{T}{\Theta}\right)^3 \int_0^{\Theta/T} \frac{x^2 dx}{e^x - 1}. \tag{4}$$

As the the phonon term is linear above the Debye temperature ($\Theta \approx 210$ K),[6] the strength of phonon scattering, a_1, can be determined from the high temperature slope of the zero field resistivity curves. The calculated $\rho_{\mathrm{ph}}(T)$ curves are shown by dashed lines in the upper panel of Fig. 7. The difference of the total resistivity and its phonon related part is attributed to the magnetic scattering, and $\rho_0+\rho_{\mathrm{magn}}(T,0)$ is displayed in Fig. 7(a) by dotted line. As it was expected, the magnetic scattering is temperature independent at high temperatures over several hundreds of Kelvin. The magnetic scattering decreases gradually as the blocking temperature is approached from above, but at $T=4.2$ K there is still a considerable contribution to the resistivity, i.e., $\rho(T=4.2\ \mathrm{K}, B=0\ \mathrm{T}) \neq \rho(T=4.2\ \mathrm{K}, B=12\ \mathrm{T})$.

Since the phonon term is magnetic field independent, the $\rho_{\mathrm{ph}}(T)$ curves determined from the zero field temperature dependencies can be used to separate the magnetic scattering contribution in the high field measurements. The temperature dependence of the magnetic scattering in $B=12$ T is shown by dashed line in Fig. 7(b). It has a huge contribution to the total resistivity, it dominates over even the phonon term below $T\approx 250$ K.

At fields as high as $B=12$ T the magnetic moments of the large grains are almost completely aligned by the applied magnetic field, as it can be deduced from the magnetization data shown in Fig. 5. We assume that in this high field limit the magnetic scattering of the spin-polarized electrons is proportional to the spin disorder of the small clusters and this gives rise to the strong temperature dependence of $\rho_{\mathrm{magn}}(T, B=12\ \mathrm{T})$ separated in Fig. 7(b). The spin disorder for a characteristic moment S can be expressed by the Brillouin-function, $B_S = \langle S_z \rangle / S$:

$$\rho_{\mathrm{magn}}(T,B) = a_2(S - \langle S_z \rangle) = a_2 \left[S - \left(S + \frac{1}{2}\right) \times \coth \frac{(2S+1) g \mu_B B}{2kT} + \frac{1}{2} \coth \frac{g \mu_B B}{2kT} \right]. \tag{5}$$

Here, S and $\langle S_z \rangle$ are the total spin and its z-component of the scatterers, respectively.

The fitted $\rho_{\mathrm{magn}}(T, B=12\ \mathrm{T})$ curve is shown in Fig. 8 by

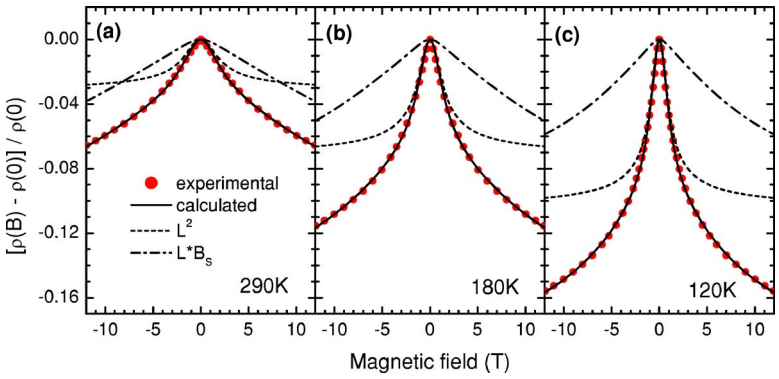

FIG. 9. (Color online) Magnetic field dependence of the resistivity in the superparamagnetic range, at various temperatures. The open symbols are experimental data, the solid line is the fit according to Eq. (7). The dashed and dash-dotted curves correspond to the first and second terms of Eq. (7), respectively. The magnetic moments of the clusters and the grains were taken from independent experiments, see text for details.

solid line. Apart from a normalization factor, a_2, the magnetic moment characteristic to the small Fe clusters is the only fitting parameter. The good agreement of the experimental and the calculated curves indicates that the size distribution of these clusters is negligible.

V. FIELD DEPENDENCE OF THE SCATTERING

In this section we demonstrate the consistency of our analysis by evaluating the magnetic field dependence of the resistivity *in the whole magnetic field range* (Fig. 9) at various temperatures in the superparamagnetic regime. For this we use the characteristic sizes determined independently from the magnetization data and from the temperature dependence of the resistivity. The Langevin fits to the SQUID magnetization experiments have shown the presence of large grains with $\mu_G \approx 500\ \mu_B$ (Fig. 4), while the temperature dependence of the resistivity in high magnetic field indicated the presence of small clusters with $S \approx 17\ \mu_B$.

Following Gittleman's model[7] we describe the magnetoresistance by the field dependence of the correlation between the localized magnetic moments responsible for an initial and a final magnetic scattering process:

$$\frac{\Delta\rho}{\rho} \propto \langle \boldsymbol{\mu}_i \boldsymbol{\mu}_f \rangle \propto \langle \boldsymbol{\mu}_i \mathbf{B} \rangle \langle \boldsymbol{\mu}_f \mathbf{B} \rangle. \quad (6)$$

In the case of the observed two largely different grain sizes this can be expressed as

$$\frac{\Delta\rho}{\rho} = -b_1 L^2\left(\frac{\mu B}{kT}\right) - b_2 L\left(\frac{\mu B}{kT}\right) B_S(B,T) - b_3 B_S^2(B,T) \quad (7)$$

where B_S is the Brillouin-function defined under Eq. (5) for the small iron clusters and $L(x)$ is the Langevin-function (i.e., the classical limit of B_S) defined under Eq. (1) for the large Fe grains. The parameters b_1, b_2, and b_3 represent the relative weights of scattering from grain to grain, between a grain and a cluster and from cluster to cluster.

Figure 9 shows the measured magnetoresistance for three selected temperatures well above the blocking temperature. The lines show the fit to Eq. (7). The two characteristic magnetic moments were fixed to the values ($\mu_G = 500\ \mu_B$ and $S = 17\ \mu_B$) determined in the previous analysis from independent experiments: The field and temperature dependence of the bulk magnetization, and the temperature dependence of the resistivity. The relative weights of the various processes were used as fitting parameters.

We found that b_2 (which describes the grain to cluster scattering) is temperature independent. Moreover, it agrees within 5% with a_2 introduced in Eq. (5) and determined previously from the temperature dependence of the scattering on clusters in the high magnetic field limit (see Fig. 8). This agreement confirms the consistency of our analysis. The relative weight of the grain to grain scattering process, b_1, increases with decreasing temperature and it is somewhat larger than b_2. This reflects the large probability of scattering from grain to grain due to the large volume fraction of this type of magnetic scatterer, even though the amplitude of the grain scattering is small.[5] The direct interplay between the clusters (b_3) is negligible, as expected for a small fraction (less than 2%).

In Fig. 9 the dashed and the dashed-dotted lines represent the contribution of the two dominant scattering processes. The grain to grain scattering process is the leading term in Eq. (7) at low magnetic fields. The dashed line corresponds to the square of the magnetization due to the grains, and if this were the only scattering process the simple relation[7] of $\Delta R(B) \propto M^2$ would hold. However, the second term of Eq. (7) is not negligible, and accordingly at high fields deviation from the simple quadratic behavior appears. This is clearly revealed by plotting the pure experimental data in Fig. 10.

The good description of the measured magnetization (Fig. 4) and resistance curves (Figs. 8 and 9) by two characteristic sizes is the consequence of the narrow size distributions of the grains and the clusters. Moreover the magnetic moments of the large grains and the small clusters differ more than an order of magnitude; $\mu_G \approx 500\ \mu_B$, and $S \approx 17\ \mu_B$, and according to the Mössbauer spectroscopy measurements the small clusters contain only a small fraction (below 2%) of the magnetic atoms. This explains why the bulk magnetization is determined by the properties of the large grains at all temperatures, while in the transport properties the magnetic scattering of small clusters plays an important role.

VI. GRANULAR MULTILAYERS WITH DIFFERENT SPACER THICKNESS

The simple description of the magnetic properties in the framework of an interaction-free superparamagnetic model with uniform grains certainly does not work for small spacer

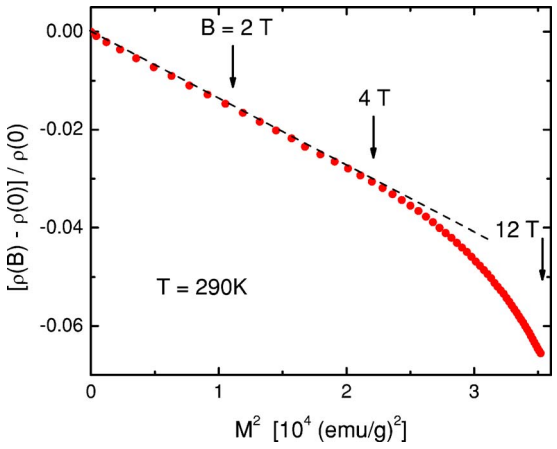

FIG. 10. (Color online) Magnetoresistance vs the square of the magnetization in the superparamagnetic range (data taken from Figs. 5 and 9). Deviation from the simple $\Delta R(B) \propto M^2$ quadratic behavior signifies the effect of the small clusters, which barely contribute to the magnetization but dominate the scattering at high fields.

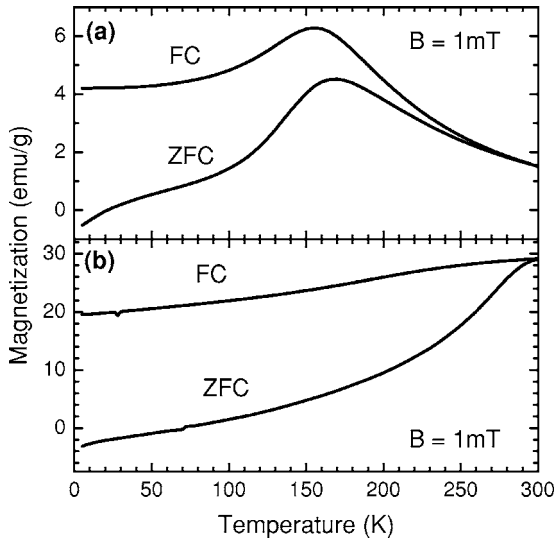

FIG. 11. Zero field cooled (ZFC) and field cooled (FC) magnetization as a function of temperature for smaller spacer thickness (samples B and C).

thickness (i.e., for large Fe concentrations). The effect of grain size distribution and increasing strength of interaction between the grains are studied on two further samples, where the Ag layer thickness is decreased:

$$\text{(B) } [\text{Ag}(1.3\text{ nm})/\text{Fe}(0.2\text{ nm})]_{75}/\text{Ag}(1.3\text{ nm})$$

$$\text{(C) } [\text{Ag}(0.8\text{ nm})/\text{Fe}(0.2\text{ nm})]_{75}/\text{Ag}(0.8\text{ nm}).$$

The relation between the size of the grains in granular multilayers and the nominal layer thickness is generally determined by a three-dimensional growth process.[25] The average diameter of the grains can be much larger than the nominal layer thickness, depending on the material parameters (e.g., lattice parameter mismatch, surface energy, etc.), as well as various parameters (deposition rate, substrate temperature, etc.) of the deposition technique.

The increase of the spacer layer thickness from 2.6 to 5.4 nm was found[20] to decrease the magnetic grain size in Fe-Ag granular multilayer samples. For samples B and C where the spacer layer thickness is decreased below 2.6 nm the magnetic grain size is expected to increase according to this trend and also due to an increasing number of the pinholes and discontinuities of the spacer.

The FC-ZFC magnetization curves of samples B and C are shown in Fig. 11. The smeared curves and the increased irreversibility temperatures indicate a broad grain size distribution, but interactions between the grains are also likely to play a role[11,26,27] as the Fe concentration increases. The magnetoresistance curves (Fig. 12) show qualitative trends that are quite general for granular alloys with increasingly large concentration of the magnetic component:[3,15,28,29] the larger the Fe concentration (i) the smaller the magnetorsistance at 4.2 K, and (ii) the more sluggish the temperature dependence of the magnetoresistance. For the present case these trends even result in a reversal of the order of the magnetoresistance curves between T=4.2 K and T=290 K. (This property of Fe/Ag multilayers have already been observed,[30] but the interpretation was different.) The shape of the magnetoresistance curves of samples B and C are also very different in small fields at 290 K. A linear variation of the magnetoresistance is expected[8] when part of the grains are ferromagnetic or in a blocked state.

On one hand, it is obvious that we cannot attempt to describe the field dependence of the magnetoresistance with the simple model applied for sample A. On the other hand, the nonsaturating magnetoresistance is clearly present in these samples, as well, even though both the increasing grain size and the interaction between the grains would favor an easier alignment of the magnetic moments. The temperature depen-

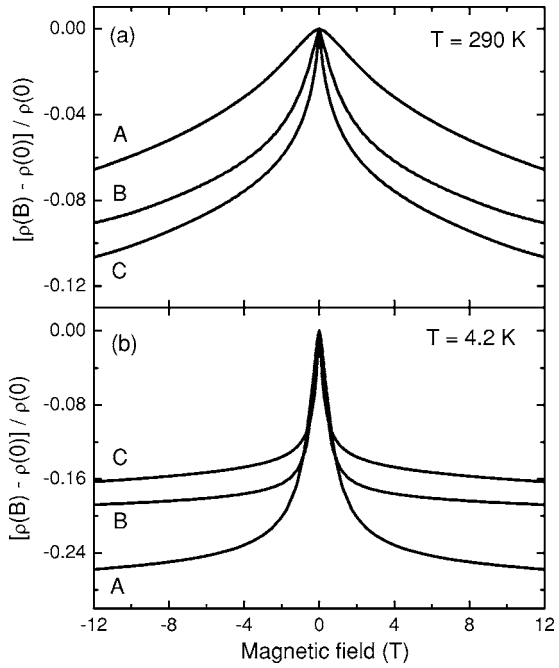

FIG. 12. Magnetoresistance of samples A–C at room temperature (a) and at T=4.2 K (b).

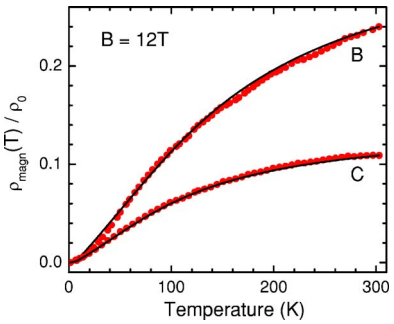

FIG. 13. (Color online) Temperature dependence of the resistivity contribution attributed to magnetic scattering on tiny Fe clusters for samples B and C. Symbols are the high field experimental data after subtracting the phonon contribution, solid curves are calculated from Eq. (5).

dence of the resistivity in $B=0$ and 12 T field was also measured for samples B and C. A similar analysis as described for sample A provided the temperature dependence of the magnetic scattering, as shown in Fig. 13. Fitting these curves by Eq. (5) gave $S=17.0$ and 12.5 μ_B cluster moments for samples B and C, respectively, quite close to the value deduced for sample A.

Bimodal distribution of the grain size has already been observed in granular systems prepared by codeposition,[10,31,32] rapid quenching from the melt,[33] or layered growth[34,35] of the constituents. Since for our samples a nonsaturating magnetoresistance indicates the presence of small clusters even in case of 25 nm thick continuous Fe layers,[36] we associate the large grains and the small clusters to Fe rich grains of the granular layers and small Fe clusters trapped inside the Ag matrix either in between the large Fe grains or inside the Ag layers, respectively. Intermixing of the layers can occur during the sample growth even when the heat of mixing is positive,[23] like in the case of Fe and Ag. On the other hand, the tendency for nonequilibrium mixing does not seem to depend on the sample preparation method, since the magnetoresistance and the magnetic properties of our granular multilayers are very similar to those observed in codeposited samples.[37,38]

VII. SUMMARY

In conclusion, we investigated the magnetic properties of sequentially evaporated granular Fe-Ag films. Unusual magnetotransport features (like sublinear temperature dependence of the resistivity over a wide temperature range both in zero and 12 T magnetic fields and large, nonsaturating GMR) were found experimentally. The contribution of the magnetic scattering was separated and analyzed. The data suggest a granular system with bimodal size distribution of the magnetic components: Coexisting large grains and small clusters. A detailed numerical analysis was given to determine characteristic grain- and cluster-moments, and their influence both on the scattering processes and on the macroscopic magnetization. The analysis reveals that scattering on the small clusters plays a dominant role in the magnetoresistance at high magnetic fields over a wide temperature range.

ACKNOWLEDGMENTS

We are grateful to J. Swerts for growing the multilayer sample examined by electron microscopy. Financial support of the Hungarian Scientific Research Fund under Grant Nos. TS049881, T034602, and T038383 are acknowledged.

[1] M. N. Baibich, J. M. Broto, A. Fert, F. Nguyen Van Dau, F. Petroff, P. Etienne, G. Creuzet, A. Friederich, and J. Chazelas, Phys. Rev. Lett. **61**, 2472 (1988).
[2] T. Valet and A. Fert, Phys. Rev. B **48**, 7099 (1993).
[3] A. E. Berkowitz, J. R. Mitchell, M. J. Carey, A. P. Young, S. Zhang, F. E. Spada, F. T. Parker, A. Hutten, and G. Thomas, Phys. Rev. Lett. **68**, 3745 (1992).
[4] J. Q. Xiao, J. S. Jiang, and C. L. Chien, Phys. Rev. Lett. **68**, 3749 (1992).
[5] S. Zhang and P. M. Levy, J. Appl. Phys. **73**, 5315 (1993).
[6] A. Milner, I. Ya. Korenblit, and A. Gerber, Phys. Rev. B **60**, 14821 (1999).
[7] J. I. Gittleman, Y. Goldstein, and S. Bozowski, Phys. Rev. B **5**, 3609 (1972).
[8] B. J. Hickey, M. A. Howson, S. O. Musa, and N. Wiser, Phys. Rev. B **51**, R667 (1995).
[9] E. F. Ferrari, F. C. S. da Silva, and M. Knobel, Phys. Rev. B **56**, 6086 (1997).
[10] J. F. Gregg, S. M. Thompson, S. J. Dawson, K. Ounadjela, C. R. Staddon, J. Hamman, C. Fermon, G. Saux, and K. O'Grady, Phys. Rev. B **49**, 1064 (1994).
[11] D. Kechrakos and K. N. Trohidou, Phys. Rev. B **62**, 3941 (2000).
[12] P. Allia, M. Coisson, P. Tiberto, F. Vinai, M. Knobel, M. A. Novak, and W. C. Nunes, Phys. Rev. B **64**, 144420 (2001).
[13] J. Balogh, D. Kaptás, T. Kemény, L. F. Kiss, T. Pusztai, and I. Vincze, Hyperfine Interact. **141**, 13 (2002).
[14] M. Rubinstein, J. Tejada, and X. X. Zhang, J. Appl. Phys. **75**, 6557 (1994).
[15] E. A. M. van Alphen and W. J. M. de Jonge, Phys. Rev. B **51**, 8182 (1995).
[16] D. Babonneau, F. Petroff, J. L. Maurice, F. Fettar, and A. Vaurés, Appl. Phys. Lett. **76**, 2892 (2000).
[17] T. L. Hylton, K. R. Coeffy, M. A. Parker, and J. K. Howard, Science **261**, 1021 (1993).
[18] S. Yamamuro, T. Hihara, K. Wakoh, T. J. Konno, K. Sumiyama, and K. Suzuki, Mater. Sci. Eng., A **217/218**, 336 (1996); C. Peng, S. Zhang, G. Li, and D. Dai, J. Appl. Phys. **76**, 998 (1994).
[19] J. Q. Wang and G. Xiao, Phys. Rev. B **49**, 3982 (1994).
[20] J. Balogh, D. Kaptás, L. F. Kiss, T. Pusztai, E. Szilágyi, Á. Tunyogi, J. Swerts, S. Vandezande, K. Temst, and C. Van Haesendonck, Appl. Phys. Lett. **87**, 102501 (2005).
[21] K. Sumiyama, Vacuum **41**, 1211 (1990).
[22] I. Vincze, Solid State Commun. **25**, 689 (1978).
[23] D. E. Bürgler, C. M. Schmidt, D. M. Schaller, F. Meisinger, R. Hofer, and H. J. Güntherodt, Phys. Rev. B **56**, 4149 (1997).

[24] Note that similar behavior was found found in Fe-Ag co-deposited granular films (Ref. 37) as well as in many other systems (for a review see Ref. 28).
[25] I. Daruka and A. L. Barabási, Phys. Rev. Lett. **79**, 3708 (1997).
[26] R. W. Chantrell, N. Walmsley, J. Gore, and M. Maylin, Phys. Rev. B **63**, 024410 (2001).
[27] C. Binns, M. J. Maher, Q. A. Pankhurst, D. Kechrakos, and K. N. Trohidou, Phys. Rev. B **66**, 184413 (2002).
[28] X. Batlle and A. Labarta, J. Phys. D **35**, R15 (2002).
[29] F. Spizzo, E. Angeli, D. Bisero, F. Ronconi, P. Vavassori, P. Allia, V. Selvaggini, M. Coisson, P. Tiberto, and F. Vinai, J. Magn. Magn. Mater. **262**, 88 (2003).
[30] C. Yu, S. Li, W. Lai, M. Yan, Y. Wang, and Z. Wang, Phys. Rev. B **52**, 1123 (1995).
[31] V. Franco, X. Batlle, and A. Labarta, J. Appl. Phys. **85**, 7328 (1999).
[32] Yu. G. Pogorelov, G. N. Kakazei, J. B. Sousa, A. F. Kravets, N. A. Lesnik, M. M. Pereira de Azevedo, M. Malinowska, and P. Panissod, Phys. Rev. B **60**, 12200 (1999).
[33] B. J. Hickey, M. A. Howson, S. O. Musa, G. J. Tomka, B. D. Rainford, and N. Wiser, J. Magn. Magn. Mater. **147**, 253 (1995).
[34] F. Nouvertné, U. May, M. Bamming, A. Rampe, U. Korte, G. Güntherodt, R. Pentcheva, and M. Scheffler, Phys. Rev. B **60**, 14382 (1999).
[35] D. Venus, F. Hunte, I. N. Krivorotov, T. Gredig, and E. Dan Dahlberg, J. Appl. Phys. **93**, 8609 (2003).
[36] J. Balogh, L. F. Kiss, A. Halbritter, I. Kézsmárki, and G. Mihály, Solid State Commun. **122**, 59 (2002).
[37] S. A. Makhlouf, K. Sumiyama, and K. Suzuki, Jpn. J. Appl. Phys., Part 1 **33**, 4913 (1994).
[38] J-Q. Wang and G. Xiao, Phys. Rev. B **49**, 3982 (1994).